

# Size-Resolved Density Measurements of Particle Emissions from an Advanced Combustion Diesel Engine: Effect of Aggregate Morphology

Teresa L. Barone,<sup>†</sup> Anshuman A. Lall,<sup>†,§</sup> John M. E. Storey,<sup>†</sup> George W. Mulholland,<sup>§,||</sup> Vitaly Y. Prikhodko,<sup>†</sup> Jennifer H. Frankland,<sup>†</sup> James E. Parks,<sup>†</sup> and Michael R. Zachariah<sup>\*,§,||</sup>

<sup>†</sup>Fuels, Engines and Emissions Research Center, Oak Ridge National Laboratory, NTRC Building, 2360 Cherahala Boulevard, Knoxville, Tennessee 37932, United States

<sup>§</sup>University of Maryland, College Park, Maryland 20742, United States

<sup>†</sup>Department of Mechanical Engineering, Vanderbilt University, Olin Hall Room 101, 2400 Highland Avenue, Nashville, Tennessee 37212, United States

<sup>||</sup>National Institute of Standards and Technology, Gaithersburg, Maryland 20899, United States

**ABSTRACT:** We report the first in situ size-resolved density measurements of particles produced by premixed charge compression ignition (PCCI) combustion and compare these with conventional diesel exhaust particles. The effective densities ( $\rho_{\text{eff}}$ ) of size-classified particles were determined by measurements with a differential mobility analyzer (DMA) and an aerosol particle mass analyzer (APM). Particle inherent densities ( $\rho_i$ ) were calculated using an expression for particle mass given by idealized aggregate (IA) theory, transmission electron microscopy (TEM) measurements of primary particle diameter ( $d_{\text{pp}}$ ), and a comparison of the measured number of particles in each size class with that predicted by a proposed DMA-APM response function for aggregates. The  $\rho_{\text{eff}}$  of PCCI and conventional diesel particles were similar over a range of diameters characteristic of their number-size distributions. The  $\rho_{\text{eff}}$  were 0.89, 0.58, and 0.51 g/cm<sup>3</sup> for conventional diesel and 0.90, 0.62, and 0.42 g/cm<sup>3</sup> for PCCI particles with 50, 100, and 150 nm electrical mobility diameters ( $d_m$ ), respectively. The error associated with  $\rho_{\text{eff}}$  was about one percent of each measurement. The lowest  $\rho_{\text{eff}}$  were observed for exhaust gas recirculation (EGR) levels somewhat lower than that required for PCCI operation. The  $\rho_i$  of 50 and 100 nm conventional diesel particles were  $1.22 \pm 0.14$  and  $1.77 \pm 0.29$  g/cm<sup>3</sup>, which is in good agreement with previously reported values. PCCI  $\rho_i$  for these size classes did not differ significantly ( $1.27 \pm 0.16$  and  $2.10 \pm 0.20$  g/cm<sup>3</sup>), suggesting like amounts of adsorbed liquid hydrocarbons. In addition, for 150 nm particles, the PCCI and conventional  $\rho_i$  were the same ( $2.20 \pm 0.34$  g/cm<sup>3</sup>). Given the close density values, we expect that particulate emissions control with diesel particulate filters (DPFs) would not be adversely affected by PCCI particle physical properties.

## INTRODUCTION

The morphology of nanoparticles may affect soot layer porosity within diesel particulate filters (DPFs). A recently published model on the influence of morphology suggests aggregates form more porous layers than single nanoparticles upon deposition over a wide range of flow conditions; in addition, particles which are more fractal-like form more porous layers for both convection- and diffusion-dominated deposition.<sup>1</sup> Changes to soot layer porosity can alter mass, heat, and momentum transfer with the exhaust gases. In particular, low soot-layer porosity may cause high regeneration temperatures and exhaust backpressure on the engine, which can lead to DPF substrate damage and reduced fuel efficiency.<sup>2</sup> Thus the particle emissions characteristics of advanced combustion strategies such as homogeneous charge compression ignition (HCCI) and premixed charge compression ignition (PCCI) should be studied considering the possible influence on DPF performance.

For PCCI combustion, fuel and air are mixed before ignition as in gasoline engines, and the combustion event is controlled by compression ignition as in diesel engines. These features enable reduced soot formation while maintaining engine efficiency.<sup>3,4</sup> In addition, high exhaust gas recirculation (EGR) is used to lower the peak combustion temperature for reduced NO<sub>x</sub> emissions.<sup>5,6</sup>

High EGR ratios and premixed fuel and air, characteristic of advanced combustion, affect the particle size distribution,<sup>7</sup> for example, with PCCI combustion near idle (1500 rpm and 0.8 bar) on a light-duty engine, the geometric mean diameter of the size distribution was half of the conventional diesel value, and the number concentration was 40% less.<sup>8</sup>

Although the particle diameter and number concentration emissions may decrease with PCCI combustion, the soluble organic fraction (SOF) present on soot can increase.<sup>8</sup> This introduces the question of whether the soot is dry or coated/encapsulated in an organic liquid layer while suspended in the exhaust, which would change the particle effective density ( $\rho_{\text{eff}}$ ). An organic liquid layer on conventional diesel engine-emitted soot<sup>9</sup> has not been observed by electron microscopy analysis in the peer-reviewed literature to the authors' knowledge.<sup>10–12</sup> However, it is possible to image a liquid layer on soot by electron microscopy as shown in atmospheric investigations.<sup>13–15</sup> Some studies suggest that most adsorbed organics on conventional diesel engine-emitted soot may be located

Received: January 15, 2011

Revised: March 27, 2011

Published: March 30, 2011

in the primary particle pores and not largely influence primary particle and aggregate diameter.<sup>16,17</sup> However, it is still to be determined whether PCCI particles are encapsulated by a liquid layer, or other changes in morphology have occurred along with alteration of the particle size distribution.

The presence of organic liquid on a soot particle would increase the particle mass while marginally affecting the particle diameter.<sup>16</sup> Since the particle mass is influenced, so might be the  $\rho_i$  and  $\rho_{\text{eff}}$ . The  $\rho_i$  is the composite material density of the solid and liquid species that compose each primary particle of a nanoparticle aggregate and was first measured for conventional diesel soot by Park et al.<sup>18</sup> It can be calculated as the particle mass ( $m$ ) divided by the sum of the primary particle volumes ( $\Sigma V_{\text{pp}}$ )

$$\rho_i = \frac{m}{\Sigma V_{\text{pp}}} = \frac{m}{\frac{\pi}{6} N_p d_{\text{pp}}^3} \quad (1)$$

where  $\Sigma V_{\text{pp}}$  is the product of the average  $d_{\text{pp}}$  and the number of primary particles ( $N_p$ ). Park et al.<sup>2</sup> estimated  $N_p$  using TEM measurements of aggregate projected area. The image processing and analysis for this measurement can be time-consuming, so we propose an alternative method to calculate  $\rho_i$  using IA theory and the DMA-APM transfer function. IA theory provides a relationship between particle morphology and mobility based on an analysis of nanoparticle aggregate transport in the free-molecular ( $d_{\text{pp}} < \text{gas mean free path } (\lambda)$ ) and transition ( $d_{\text{pp}} \approx 2\lambda$ ) regimes.<sup>19</sup> For the analysis, it is assumed that  $d_{\text{pp}}$  is uniform and most primary particles are exposed to collisions with the surrounding gas molecules, which is a good approximation for fractal dimensions less than 2.  $N_p$  is related to  $d_m$  by IA theory as follows:<sup>20–22</sup>

$$\frac{d_m}{C(d_m)} = \frac{c^* N_p d_{\text{pp}}^2}{12\pi\lambda} \quad (2)$$

where  $C(d_m)$  is the slip correction factor<sup>23</sup> and  $c^*$  is a constant that appears in the friction factor given by Dahneke.<sup>24</sup> An appropriate correction for primary particles in the transition regime can be applied.<sup>19,24</sup> Next combining eq 1 and eq 2,  $m$  is expressed in terms of  $\rho_i$ ,  $d_{\text{pp}}$ , and  $d_m$ .

$$m = \frac{2\pi^2\lambda d_{\text{pp}}}{c^*} \frac{d_m}{C(d_m)} \rho_i \quad (3)$$

Finally,  $\rho_i$  is calculated iteratively such that the mass-dependent DMA-APM transfer function based on theory best fits the transfer function based on the measured data. The DMA-APM transfer function based on theory was modified for particles with aggregate morphology in the current study and this development is given in the next section.

The  $\rho_{\text{eff}}$  is used to quantify the density of irregularly shaped particles and is given by the quotient of  $m$  and the volume based on  $d_m$  ( $V_{\text{mobility}}$ ).

$$\rho_{\text{eff}} = \frac{m}{V_{\text{mobility}}} \quad (4)$$

To obtain  $\rho_{\text{eff}}$ , we measured  $d_m$  using the DMA, calculated  $V_{\text{mobility}}$ , and measured  $m$  using the APM. If soot were spherical,  $\rho_i$  and  $\rho_{\text{eff}}$  would be equal. However, soot is largely present as nanoparticle aggregates, for which  $\Sigma V_{\text{pp}}$  is often lower than  $V_{\text{mobility}}$ .<sup>10,20</sup> Thus  $\rho_{\text{eff}}$  is usually less than  $\rho_i$ . In addition,  $\rho_{\text{eff}}$  can be lower than the density of organic liquids ( $\sim 0.8 \text{ g/cm}^3$ ),<sup>25</sup> which is the approximate density of hydrocarbons with high carbon number that display properties of a subcooled liquid when

adsorbed on soot.<sup>26–28</sup> In the absence of any adsorbed or coating liquid,  $\rho_i$  was found to be independent of particle diameter and have value  $1.77 \text{ g/cm}^3$  for conventional diesel particles.<sup>18</sup>

In the current study, PCCI  $\rho_{\text{eff}}$  and  $\rho_i$  were compared to that of conventional diesel soot for 50, 100, and 150 nm  $d_m$ . This is of current interest since the particle density influences the soot layer porosity within a DPf, which in turn affects DPf performance. In addition, information on particle densities and/or comparison with reference soot of known composition is widely desired for improved understanding of particulate emission data obtained by routinely used aerosol instruments, such as the DMA. For example, the particle number distributions measured by the DMA can be converted to mass distributions if the size-dependent  $\rho_{\text{eff}}$  is known.

## THEORY

**DMA-APM Response Function for Aggregates.** A combination of a DMA and an APM is often used to measure mass of the mobility-classified particles.<sup>10,22,29–32</sup> A detailed model for inverting the output of the DMA-APM system to determine the input size distribution was previously developed by Emery.<sup>33</sup> His analysis was analogous to that of a tandem-DMA (DMA-DMA) response function.<sup>34,35</sup>

Lall et al.<sup>29</sup> suggested a simpler method to describe the combined DMA-APM response function. A mobility distribution with the same shape as the DMA transfer function was chosen, and the APM response function resulting from the known distribution was calculated. The DMA transfer function is a triangular function in terms of electrical mobility and can be approximated as a distorted triangular function for narrow distributions. The calculations were compared with measurements made with NIST Standard Reference Materials (SRM) polystyrene latex (PSL) spheres. The measured modal diameter ( $\pm$  uncertainty based on 95% confidence) for the SRM PSL particles were previously reported as  $60.39 \pm 0.69 \text{ nm}$  and  $100.7 \pm 1.0 \text{ nm}$ .<sup>36</sup> Because these particles have high accuracy for the mode diameter, Lall et al.<sup>29</sup> were able to assess the accuracy of the APM mass measurement for spheres. To fully understand APM accuracy for nanoparticle aggregates, properties such as fractal dimension,  $N_p$  and  $d_{\text{pp}}$  should be systematically controlled and investigated, which is beyond the scope of the present study. However, in a step toward understanding DMA-APM classification of particles with aggregate morphology, the instrument response for ideal aggregates is predicted and compared with measured data.

We extend the method of Lall et al.<sup>29</sup> to include the effect of aggregate morphology in the DMA-APM transfer function for the characterization of diesel and PCCI soot. This is presented in the following analysis for a narrow triangular particle size distribution, which nominally represents mobility classified particles from a DMA. Let  $G(d_m)$  be a triangular function, which approximately resembles the DMA transfer function, such that it can be used to describe the number-size distribution of particles exiting the DMA

$$dN = G(d_m) dd_m \quad (5)$$

where  $N$  is particle number concentration and

$$G(d_m) = \Omega_{\text{DMA}}(d_m) n(d_m) = \Omega_{\text{DMA}}(d_m) \left( \frac{N_0}{\Delta d_m} \right) \quad (6)$$

where  $\Omega_{\text{DMA}}$  is the DMA transfer function and  $n(d_m)$  is the particle size distribution that enters the DMA. All particles are

assumed singly charged. For the narrow range of mobility diameters considered in our analysis, we approximated  $n(d_m)$  by a constant function,  $N_0/\Delta d_m$ , where  $N_0$  is the total concentration of singly charged particles that enter the DMA column and  $\Delta d_m$  the full base width of triangular function  $G(d_m)$  given by

$$\Delta d_m = d_{m,\min} - d_{m,\max} \quad (7)$$

where  $d_{m,\min}$  and  $d_{m,\max}$  are the minimum and maximum mobility diameter particles sizes. It is assumed that for diesel aggregates generated in our study, the size distribution is much wider compared to the spread due to the width of the DMA transfer function. The width of the triangular function is determined by the ratio of sheath to aerosol flow rate similar to the case of DMA transfer function. The total number of particles exiting the DMA is equal to the area of the triangle. The mode of the particle size distribution is set equal to the mobility diameter.

The above-mentioned particle size distribution is divided into infinitesimal-size bins for which the APM transfer function is calculated. Thus the number of particles in each bin that exit the APM at a given voltage is determined, and the *total* number of particles that exit the APM at a given voltage is summed over each bin. The APM transfer function for particles of mass,  $m$ , and at a fixed voltage,  $V$ , is given by  $\Omega_{\text{APM}}(V, m)$ .

$$\Omega_{\text{APM}}(V, m) = \frac{n_{\text{out}}(V, m)dm}{n_{\text{in}}(m)dm} \quad (8)$$

Next, we make the following assumptions for a given narrow range of mobility diameters:

- The inherent density of the primary particles is constant.
- The size of the primary particles that compose the aggregates is uniform.
- Each aggregate carries a unit charge.
- The conditions for idealized aggregates are met such that, the  $d_m$  is related to  $N_p$  (eq 2).

Using the above assumptions, the mass of an aggregate can be calculated from  $d_m$  and  $d_{pp}$  as mentioned in the Introduction (eq 3). Thus, the APM transfer function can be expressed in terms of  $d_m$  and the number of particles exiting the APM ( $dN_{\text{out}}(V, d_m)$ ) is as follows:

$$dN_{\text{out}}(V, d_m) = \Omega_{\text{APM}}(V, d_m)dN_{\text{in}}(d_m) \quad (9)$$

where  $dN_{\text{in}}(d_m)$  is given by eq 5.

The total number concentration of particles that exit the APM at a given voltage is given by

$$N_{\text{out}}(V) = \left(\frac{N_0}{\Delta d_m}\right) \int_{d_{m,\min}}^{d_{m,\max}} \Omega_{\text{APM}}(V, d_m) \cdot \Omega_{\text{DMA}}(d_m) dd_m \quad (10)$$

Equation 10 is similar to Emery's<sup>33</sup> expression for the convolution of the DMA and APM transfer functions for spherical particles with diameter  $d_m$ . To calculate  $N_{\text{out}}(V)$  from eq 10, a previously derived expression for the APM transfer functions is used:<sup>29</sup>

$$\Omega_{\text{APM}}(V, m) = \frac{\int_{r_1}^{r_2} p(V, m, r)v(r)dr}{\int_{r_1}^{r_2} v(r)dr} \quad (11)$$

where  $p(V, m, r)$  is equal to 1 if a particle of mass  $m$  enters the APM annular region at radial position  $r$  and exits at voltage  $V$ . The value

of  $p(V, m, r)$  is equal to 0 otherwise. The parameter  $v(r)$  is the gas velocity in the annular region of the APM for an assumed laminar parabolic flow.

The effect of Brownian diffusion is included in the APM transfer function using a Monte Carlo method to calculate particles trajectories as follows:

$$r(t + \Delta) - r(t) = \frac{m\omega^2 r(t)}{(m/\tau)} \cdot \Delta - \frac{1}{(m/\tau)} \frac{qV}{r(t) \ln\left(\frac{r_2}{r_1}\right)} \cdot \Delta + (\sqrt{2D\Delta})B_x(t) \quad (12)$$

$$z(t + \Delta) - z(t) = v\Delta + (\sqrt{2D\Delta})B_z(t) \quad (13)$$

where  $r$  is the distance from the center of the concentric cylinders of the APM to the particle,  $r_1$  is the distance from the center to the outer surface of cylinder 1,  $r_2$  is the distance to the inner surface of cylinder 2, and  $z$  is the vertical position of the particle in the annulus of length  $L$ ;  $B_x(t)$  and  $B_z(t)$  are Gaussian random variables with zero mean, and standard deviation (or variance) equal to unity. The method was also previously used for both the DMA<sup>36</sup> and APM transfer functions.<sup>37</sup> In the current study, we calculate  $N_{\text{out}}(V)$  (eq 10) for an assumed  $\rho_i$ . Then we compare the calculated and measured  $N_{\text{out}}(V)$ ; the two should match if the assumed value of  $\rho_i$  is correct. The best match between the calculated and measured  $N_{\text{out}}(V)$  is found iteratively, and the corresponding inherent density is reported. The peak voltage of the calculated DMA-APM response function is also reported but was not needed to calculate the mass.

In many cases, the measured DMA-APM transfer function resembles a Gaussian function. The corresponding peak of the Gaussian function fit can be used to calculate mass using

$$mr\omega^2 = \frac{V}{r \ln(r_2/r_1)} \quad (14)$$

where  $r$  is the particle location relative to the axis of rotation,  $r_1$  and  $r_2$  are the radii of the inner and outer electrodes, respectively, and  $\omega$  is the particle angular velocity. In this study, the measured response function resembled the Gaussian distribution, and so we reported the Gaussian peak voltages also.

## EXPERIMENTAL SECTION

We evaluated the size-resolved  $\rho_{\text{eff}}$  by first classifying particles based on  $d_m$  using a DMA and determining  $V_{\text{mobility}}$ . Then, the mass of mobility-selected particles was measured by an APM, and the characteristic mass was determined from the combined DMA-APM response function. The measured response function was compared to that based on theory, which was first developed for spherical particles<sup>29</sup> and modified in the present work to account for aggregate morphology with IA theory. Finally,  $\rho_{\text{eff}}$  was calculated from the above mass and volume measurements. In addition,  $\rho_i$  was determined using IA theory and measurements of  $d_{pp}$  obtained by TEM and image analysis.

**Engine Exhaust Aerosol Measurements.** A diagram of the experimental setup for the DMA-APM measurements is shown in Figure 1. For the measurements, exhaust aerosol was sampled from a common-rail diesel engine modified to enable PCCI or conventional combustion. The modifications included the addition of an electronic intake throttle, an electronically controlled high flow exhaust gas recirculation valve (in lieu of the stock vacuum-operated valve), and an EGR cooler. In addition, the

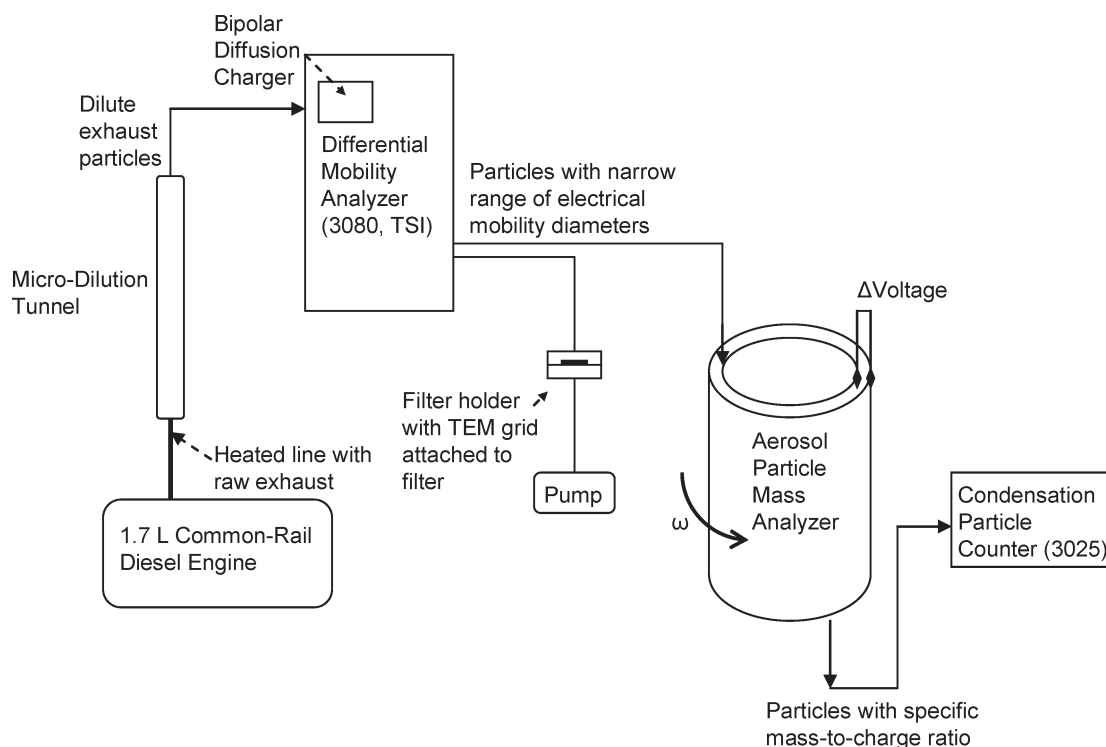


**Figure 1.** Diagram of the experimental setup for measuring diesel exhaust particle sizes and masses. Particles with a narrow range of electrical mobility diameters were passed through the aerosol particle mass analyzer for mass classification. Subsequently, at the same engine steady-state condition, the size classified particles were sampled for morphology measurements using a filter with an attached TEM grid.

factory engine control module was replaced with a rapid development engine controller based on a dSpace MicroAutoBox. This rapid development system was produced in partnership with Ricardo, Inc. and provided control over all engine electronics including timing, duration, and number of fuel-injection events. The engine is commonly used in the light-duty European Mercedes A170 and has the following specifications: 1999 model year, OM668 model number, 1.7 L displacement, 4 cylinders, 80 mm bore, and 84 mm stroke. The engine was coupled to a motoring DC dynamometer and had a rated power output of 66 kW (89 hp) at 4200 rpm. The operating conditions investigated represent near idle (1500 rpm, 0.8 bar) and a moderate cruise (1500 rpm, 2.6 bar).

A microtunnel dilution system was used to prepare exhaust aerosol samples for particle mass and size distribution measurements and is based on an ejector pump dilution design by Abdul-Khalek et al.<sup>37</sup> In the ejector pump, HEPA-filtered compressed air passes through a venturi nozzle and expands, which creates negative pressure and draws exhaust aerosol with flow rate fixed by a critical orifice into the pump. Samples were taken downstream of the engine turbocharger and transported to the pump using a heated stainless steel line at 190 °C. Exhaust and HEPA-filtered air began to mix in the ejector pump and entered the dilution tunnel, which was controlled at  $45 \pm 2$  °C. A relatively low dilution ratio of 13 was used to allow gas to particle conversion<sup>38</sup> and increase the likelihood of observing organics condensed on PCCI particles. During steady-state engine operation, number-size distributions were measured by a scanning mobility particle sizer (SMPS; model 3936, TSI Inc.), which consisted of a long DMA (model 3080, TSI Inc.) and ultrafine condensation particle counter (CPC; model 3025, TSI Inc.). The electrical mobility diameters of particles selected for subsequent

mass measurement by the APM (model 3600, Kanomax) were 50, 100, and 150 nm, which are diameters characteristic of engine-emitted nanoparticle aggregates.<sup>9</sup> For a given voltage across the APM annulus, particles with specific mass to charge ratio exited and were counted by the CPC. The APM voltage was varied and the particle number distribution was fit with the DMA-APM response function given in eq 10 and also for comparison purposes with a 3-parameter Gaussian curve.

**TEM Measurements.** The use of IA theory to calculate particle mass requires knowledge of aggregate  $d_{pp}$ , which was measured by TEM and image analysis. For the measurements, PCCI and conventional diesel particles with 50, 100, and 150 nm  $d_m$  were selected by the DMA and collected by filtration on a 300-mesh, copper TEM grid with holey carbon film (Electron Microscopy Sciences, PA) fixed to a quartz fiber filter. Forty aggregates per sampling condition were imaged at  $1.5 \times 10^5$  magnification using a Tecnai 20 TEM (FEI Co., Netherlands) in the High Temperature Materials Laboratory of Oak Ridge National Laboratory. The  $d_{pp}$ , fractal dimension, and  $N_p$  were measured using the image-analysis technique of Xiong and Friedlander.<sup>39</sup> In total, approximately 13 800 primary particles were individually measured. In addition, TEM analysis was carried out to investigate whether PCCI particles were coated or encapsulated by an organic liquid, which may be present as indicated by high SOF content.<sup>8</sup>

## RESULTS AND DISCUSSION

The  $\rho_{eff}$  and  $\rho_i$  of PCCI and conventional diesel particles were compared using DMA-APM measurements to evaluate whether PCCI particles would tend to form denser soot-cake layers when

depositing in a DPF. This is of interest since the soot cake layer density can significantly affect DPF regeneration and the exhaust backpressure on the engine.

**Particle Number-Size Distributions.** The first part of the analysis involved acquiring the number-size distribution of particles in the exhaust for PCCI and conventional diesel combustion at engine conditions representative of near idle (1500 rpm, 0.8 bar) and a moderate cruise (1500 rpm, 2.6 bar). For the near-idle condition, the PCCI particle geometric mean

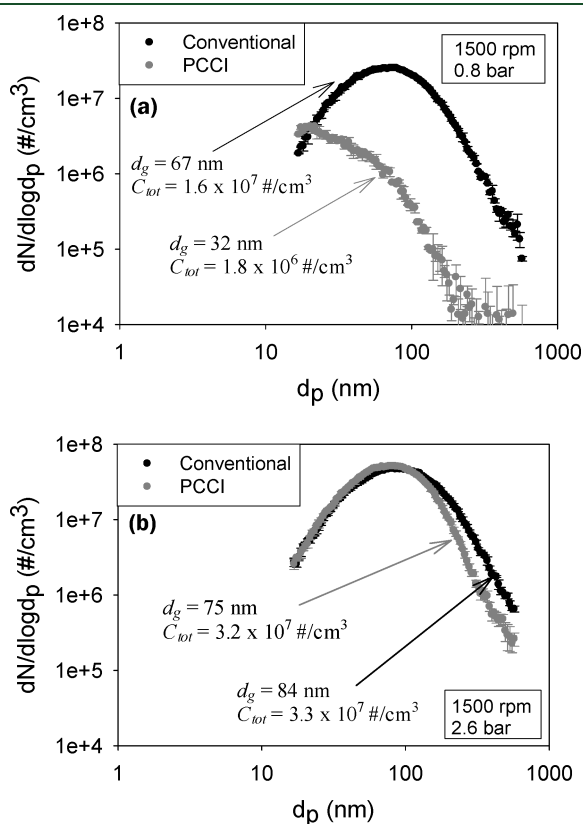


**Figure 2.** SMPS particle number-size distributions for conventional diesel and PCCI exhaust particles (a) near idle (1500 rpm, 0.8 bar) and (b) at a moderate cruise (1500 rpm, 2.6 bar). The PCCI geometric mean diameter ( $d_g$ ) and total number concentration ( $C_{tot}$ ) were less than that of conventional diesel particles, with greater difference at near idle than the moderate cruise.

diameter ( $d_g$ ; 32 nm) was less than half of that for conventional diesel particles (67 nm) (Figure 2a). Because particles with  $d_m < 16$  nm were not included in the PCCI number-size distribution measurement, the reported  $d_g$  is an upper estimate, and the actual difference between the PCCI and conventional diesel values would be greater. At the moderate cruise condition, the PCCI  $d_g$  (75 nm) was about 10 nm less than the conventional diesel particle  $d_g$  (84 nm) (Figure 2b). The results are consistent with our previous study and suggest that PCCI particle number-size distributions are skewed to the ultrafine mode.<sup>8</sup> The formation of smaller particles may be influenced by the enhanced in-cylinder fuel and air mixing enabled by early fuel injection in PCCI combustion. This reduces local in-cylinder fuel-rich zones which should prevent the formation of large aggregates. In addition, using a very high EGR ratio characteristic of PCCI combustion results in a significant reduction in the in-cylinder bulk temperature such that the formation of large aggregates is suppressed.<sup>5</sup>

The total number concentration ( $C_{tot}$ ) of PCCI particles at the near-idle condition was of order  $10^6$  no./cc, while the conventional was  $10^7$  no./cc. Because particles with  $d_m < 16$  nm were not included in the PCCI number-size distribution measurement,  $C_{tot}$  is a lower estimate, so the PCCI and conventional results would be closer. Under moderate cruise, most of the size distribution was within the instrument detection limits; the PCCI particle concentration was slightly less than or equal to the conventional. In what follows, we evaluate whether PCCI combustion can, in addition to altering the number-size distribution, change the particle effective density and morphology.

**Primary Particle Diameter Measurements.** To obtain the combined DMA-APM response function through the use of IA theory and calculate  $\rho_p$ , the average  $d_{pp}$  was determined by TEM measurements. TEM images of typical PCCI and conventional diesel aggregates are presented in Figure 3. The images were analyzed using the technique given by Xiong and Friedlander<sup>39</sup> and Barone et al.<sup>40</sup> A total of 240 aggregates and about 13 800 primary particles were analyzed for 50, 100, and 150 nm PCCI and conventional diesel particles. The mean primary particle diameters with error representing one standard deviation are given in Table 1. The results show the primary particle diameters for PCCI and conventional diesel aggregates are similar for each of the three size classes and range from 20 to 25 nm with the largest standard deviation being 4 nm. The conventional diesel results are consistent with previous measurements of aggregate primary particle diameter.<sup>13,41,42</sup> Because  $d_{pp}$  tends to increase

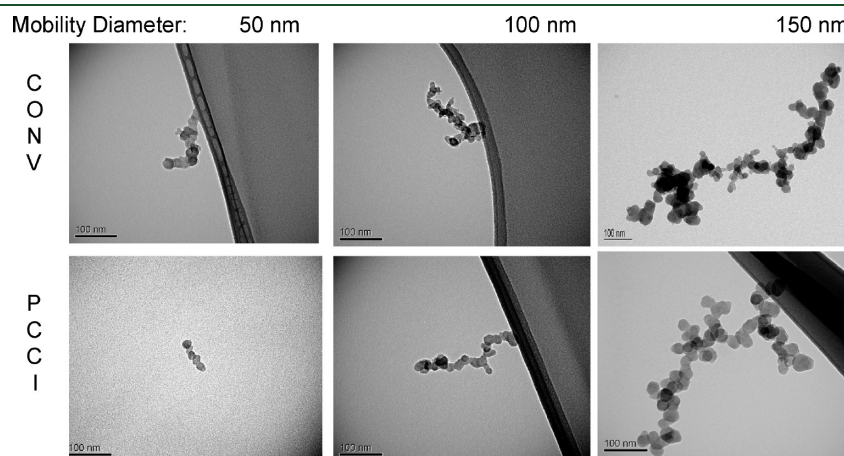


**Figure 3.** TEM images of 50, 100, and 150 nm conventional diesel and PCCI particles for the moderate cruise condition (1500 rpm, 2.6 bar).

**Table 1.** TEM Measured Primary Particle Diameter ( $d_{pp}$ ), APM Measured Peak Voltage and Calculated Mass, Idealized Volume, and Calculated Density at the Moderate Cruise Condition (1500 rpm, 2.6 bar)<sup>a</sup>

mode	mobility diameter (nm)	measured			calculated			
		$d_{pp}$ (nm)	APM peak voltage (V)		idealized volume ( $\times 10^{-23}$ m <sup>3</sup> )	mass ( $\times 10^{-20}$ kg)	inherent density (g/cm <sup>3</sup> )	effective density (g/cm <sup>3</sup> )
			Gaussian fit	response function				
conventional	50	24 ± 3	6.54	6.54	4.79	5.85	1.22 ± 0.16	0.89
	100	22 ± 4	37.27	35.4	17.4	30.8	1.77 ± 0.20	0.58
	150	25 ± 4	26.73	25.8	41.2	90.6	2.20 ± 0.29	0.51
PCCI	50	23 ± 4	6.6	6.6	4.64	5.90	1.27 ± 0.14	0.90
	100	20 ± 2	38.3	37.8	15.5	32.5	2.10 ± 0.29	0.62
	150	21 ± 3	21.53	21.6	34.0	74.8	2.20 ± 0.34	0.42

<sup>a</sup> The  $d_{pp}$  errors represent one standard deviation of the mean. The error associated with  $\rho_{eff}$  is based on the standard deviation of repeated measurements at the given engine steady-state condition and is less than or equal to 1% of the measured value.

with increasing in-cylinder fuel-rich zones,<sup>40</sup> it is surprising the conventional diesel  $d_{pp}$  was not significantly larger than the PCCI considering the enhanced fuel and air mixing with PCCI combustion.

**DMA-APM Response Function.** The size-resolved density measurements were carried out by selecting particles with a narrow range of  $d_m$  using the DMA and separating those by mass-to-charge ratio with the APM. The number concentration of particles with selected mass-to-charge ratio for given APM voltage and fixed rotational speed was measured by the CPC. The  $d_m$  selected for mass analysis were 50, 100, and 150 nm, since these are representative of the size range of PCCI and conventional diesel particles at the moderate cruise condition (1500 rpm, 2.6 bar) as shown by the SMPS number-size distribution (Figure 2b). The results for the above-described measurements are expressed as the DMA-APM response functions for PCCI (Figure 4a–c) and conventional diesel (Figure 4d–f) particles. The data were fit with a 3-parameter Gaussian curve (Figure 4), which well represented the data with  $R^2$  values of 0.95 or higher. These curves show that the particles pass through the APM at several voltages ranging from about 10 to 60 V, rather than at a single APM voltage when the centrifugal force is balanced with the electrical force (eq 14). This could be due to two reasons: (a) large spread in particle mass, at constant mobility or (b) the inherent DMA-APM response function characteristics. To investigate this issue, we compared the calculated and measured DMA-APM response functions; if the two functions match, the spread in APM voltage can be attributed to the response-function characteristic. For the comparison, particle number concentration was normalized since the measured and calculated values can differ as a result of particle losses that occur in the APM. Knowing the absolute values is not necessary since only the voltage at which the peak concentration occurs is used to determine the measured mass through eq 14. In addition, although losses in the APM are particle size-dependent, this would not affect our results because the particles were size-classified by the DMA before analysis.

We found the response function as shown in Figure 5 closely followed the measured data for 50 nm aggregates in both conventional and PCCI mode. However, the response function for the 100 nm mobility selected particles is clearly narrower than the observed distribution, which suggests a large spread in the particle mass or the presence of a non-negligible amount of compact particles which deviate from the IA model. To obtain statistically

significant measurements of fractal dimension (a measure of compactness) and estimate the deviation from the IA model, the fractal dimension of thousands of aggregates should be determined. This is very time-consuming and was not practical given our resources. Instead, we measured thousands of primary particle diameters, which is less time-consuming, and input the values into the transfer function based on IA theory. Then we compared the calculated and measured transfer functions. Despite a deviation for 100 nm, using the calculated response function to estimate  $\rho_i$  produced a reasonable value which is consistent with a previous study and will be discussed in the next section. For 150 nm (Figure 6), we found excellent agreement between the measured and calculated response functions. The agreement suggests that the  $\rho_i$  calculations based on IA theory adequately represent the measurements.

**Particle Inherent Density.** The calculated  $\rho_i$  are given in Table 1 for PCCI-mode and conventional-mode aggregates. The engine was operated at 2.6 bar (22% of rated load) in both conventional and PCCI modes. This load is representative of a moderate cruise condition, and is an operating point used in previous particle characterization studies.<sup>8,43</sup> It was found that for the conventional-mode, the  $\rho_i$  of 50, 100, and 150 nm aggregates were  $1.22 \pm 0.14$ ,  $1.77 \pm 0.29$ , and  $2.20 \pm 0.34$  g/cm<sup>3</sup>, respectively using the IA method. The uncertainty associated with  $\rho_i$  is calculated through a propagation of errors, of which the standard deviation of the measured  $d_{pp}$  is prominent. Additional uncertainties from the DMA and APM measurements depend on analyses of instrument operating parameters and particle properties, which are beyond the scope of the paper and have been investigated for spherical particles of precise diameter elsewhere.<sup>29,44</sup>

The  $\rho_i$  results for 50 and 100 nm are comparable with values found by extensive offline TEM analysis by Park et al.<sup>18</sup> The method of the current study requires less TEM analysis, since obtaining statistically significant measurements of  $d_{pp}$  (our method) is less time-consuming than whole-aggregate volumes (method of Park et al.<sup>18</sup>). Because sampling and engine parameters differed from those of Park et al.,<sup>18</sup> an exact comparison of  $\rho_i$  cannot be made. For example, a higher engine load (50% of rated) was used, which suggests that a lower concentration of hydrocarbons was present in their samples.<sup>45</sup> This could have led to less hydrocarbon adsorption and affected  $\rho_i$ .

The  $\rho_i$  for 50, 100, and 150 nm PCCI-mode aggregates were  $1.27 \pm 0.16$ ,  $2.10 \pm 0.20$ , and  $2.20 \pm 0.29$  g/cm<sup>3</sup>, respectively and thus are similar to conventional combustion (Table 1). The

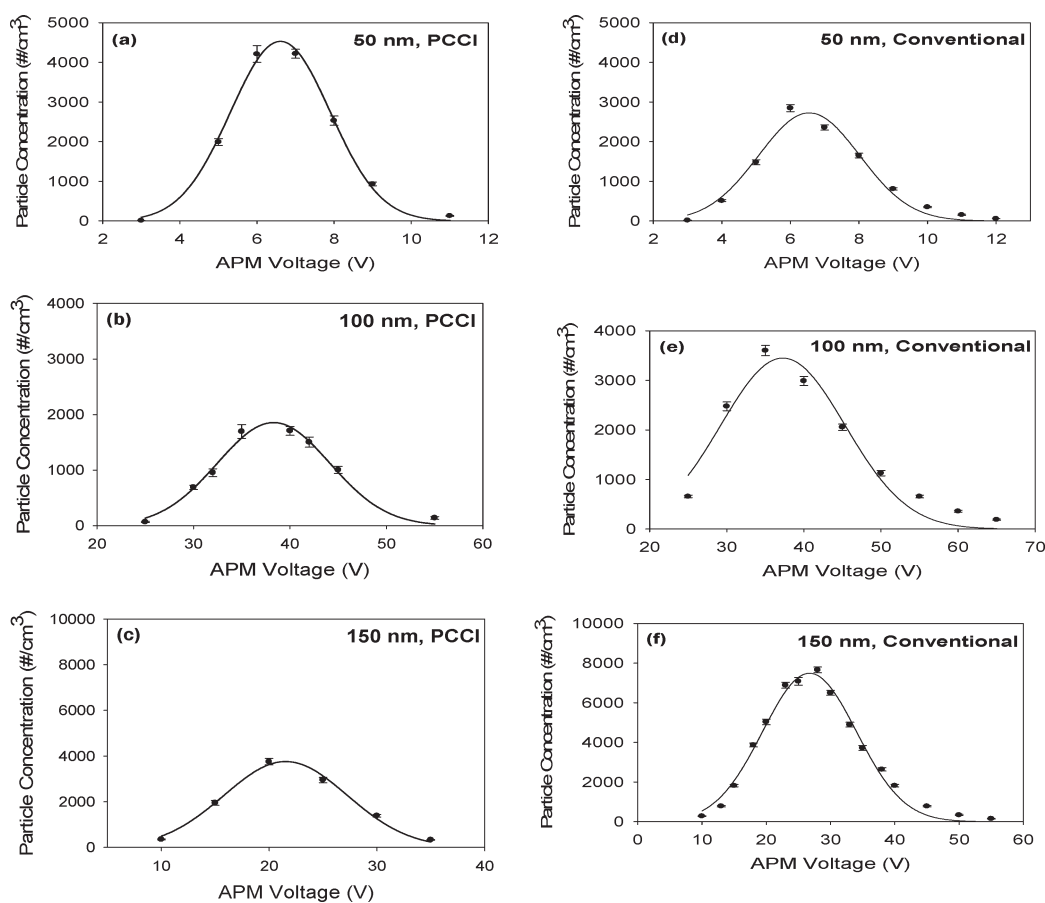


**Figure 4.** Number concentration of 50, 100, and 150 nm PCCI (a–c) and conventional diesel (d–f) particles with specific mass-to-charge ratio, which were analyzed by the APM at given voltages. The APM angular speed was fixed at 4000 rpm for all measurements except for PCCI 150 nm when it was 2000 rpm. The data were fit with 3-parameter Gaussian function.

closeness in value between PCCI and conventional  $\rho_i$  is suggestive of a similar amount of liquid hydrocarbons present as a thin surface layer and/or within the primary particle pores. Because greater particle-associated hydrocarbon content was measured for PCCI combustion previously by our group using filter-based methods,<sup>8</sup> further studies should be carried out to estimate the contribution of gas-phase heavy hydrocarbon condensation on the sample filter in the previous study. In addition, although the number concentration of particles smaller than 50 nm were equivalent for PCCI and conventional particles as shown in Figure 2b, it may be investigated in a future study as to whether the fraction of liquid droplets may be greater for PCCI in this size range and influence the larger SOF present in filter-based samples. However, at temperatures to which a DPF is exposed, liquid droplets smaller than 50 nm may be in the gas phase and not deposit on the soot layer in a DPF. In this case, the material adsorbed to soot before deposition in a DPF would be the prominent source of liquid hydrocarbons to promote enhanced oxidation. The relative amount of this adsorbed liquid is indicated by  $\rho_i$  and since it did not differ for PCCI and conventional, it would not be expected to enhance PCCI soot oxidation beyond that of conventional soot in a DPF.

**Particle Effective Density.** The  $\rho_{\text{eff}}$  of 100 and 150 nm PCCI and conventional diesel particles (Table 1) were less than the  $\rho_i$  of diesel soot (1.77 g/cm<sup>3</sup>)<sup>18</sup> and liquid organics (0.7–0.95 g/cm<sup>3</sup>). This indicates most particles were present as nanoparticle aggregates and were not encapsulated by liquid hydrocarbons.

If the aggregates were encapsulated or in other words completely immersed in liquid hydrocarbons,  $\rho_{\text{eff}}$  would be greater than or equal to the density of liquid organics. Although a thin layer of liquid hydrocarbons may be present on the aggregate surface, it probably does not affect the diameter or shape.<sup>16,17</sup> The TEM analysis results support this; most particles were present as nanoparticle aggregates with the exception of a few compact 100 nm PCCI particles such as that shown in Figure 7. Although it is possible that evaporation of organic material may have occurred in the TEM, organic droplets have been shown to survive the TEM vacuum and have been well characterized for diesel-exhaust nanoparticles.<sup>11</sup> For 50 nm PCCI and conventional diesel particles,  $\rho_{\text{eff}}$  was  $0.90 \pm 0.01$  g/cm<sup>3</sup>. The error associated with  $\rho_{\text{eff}}$  is based on the standard deviation of 150 measurements at a given engine steady-state condition and is less than or equal to 1% of the mean. The  $\rho_{\text{eff}}$  of the 50 nm particles was greater than that of the 100 and 150 nm. The larger  $\rho_{\text{eff}}$  at smaller diameter is consistent with previous studies.<sup>10,25,30,46</sup>

PCCI and conventional diesel particle masses and hence  $\rho_{\text{eff}}$  were similar for 50, 100, and 150 nm (Table 1). The similarly low  $\rho_{\text{eff}}$  values and prevalence of nanoparticle aggregate morphology observed by TEM suggest that particles produced by PCCI combustion would form layers as porous as conventional diesel soot upon deposition. Although the effects of differing flow conditions and particle diameter ranges over various speeds and

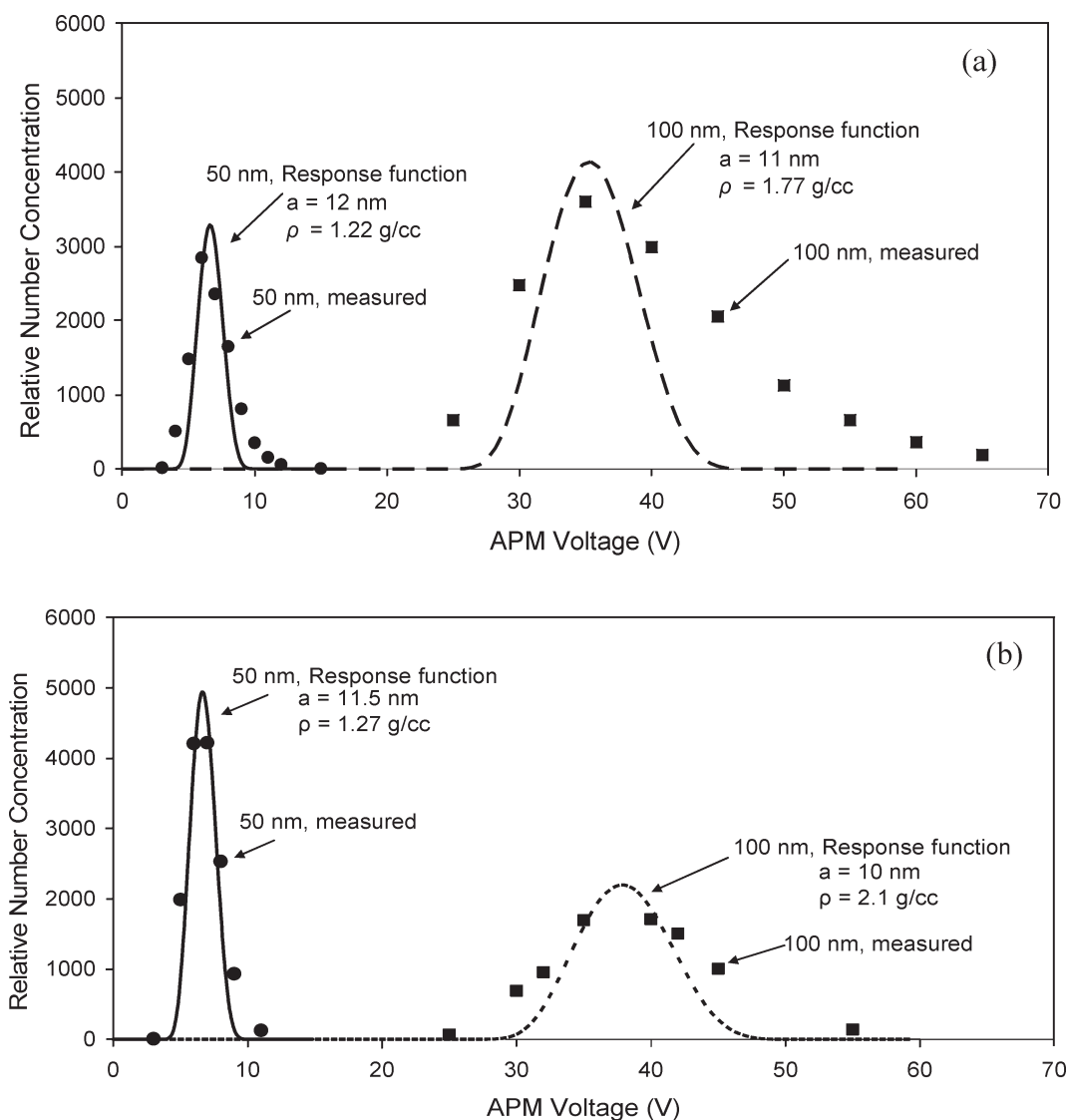


**Figure 5.** Comparison of measured and calculated DMA-APM response function for 50 and 100 nm mobility classified aggregates. The data are shown for (a) conventional mode and (b) PCCI mode. APM rotational speed = 4000 rpm. The parameter  $a$  is the primary particle radius. The height of the calculated response function is normalized for comparison. More accurate height comparison was not made in this study due to particle losses. The peak APM voltage shown above differs slightly from Gaussian fit of the measured data points shown in Figure 4. Aggregate orientation in DMA: parallel to the relative motion. Aggregate orientation in the APM is assumed random due to lesser electric field strength. Brownian diffusion is taken into account.

loads were not analyzed, the current results based on particle physical characteristics at a moderate cruise condition suggest soot layer porosity in a DPF may not be adversely affected if PCCI combustion were employed.

**Effect of EGR.** EGR is an important aspect of controlled combustion in engines. Both injection timing and EGR ratio are altered in order to switch from conventional diesel to PCCI combustion, and at intermediate points  $\text{NO}_x$  emissions decrease while the PM mass emissions increase until a plateau is reached; subsequently the PM mass drops dramatically along with  $\text{NO}_x$  emissions and PCCI combustion is achieved.<sup>47</sup> To investigate whether a change in  $\rho_{\text{eff}}$  occurs during transition to PCCI, the EGR ratio was varied, and the  $\rho_{\text{eff}}$  of particles with diameter near the geometric mean diameter of the number-size distribution was measured.

The results shown in Figure 8a show  $\rho_{\text{eff}}$  decreased from 0.72 to 0.59 g/cm<sup>3</sup> as the EGR ratio increased from 0 to 48%. At the

same time the geometric mean diameter of the number size distribution increased from 75 to 125 nm. The decrease in  $\rho_{\text{eff}}$  associated with an increase in particle diameter suggests the particles were present as nanoparticle aggregates. Advancing the EGR ratio to 51%, a value characteristic of PCCI combustion, resulted in an increase in  $\rho_{\text{eff}}$  (0.68 g/cm<sup>3</sup>) (Figure 8a), which was associated with a decrease in particle diameter (95 nm). Thus, a change in  $\rho_{\text{eff}}$  occurred upon entering into an advanced combustion regime. As shown in Figure 8b, the variation in  $\rho_{\text{eff}}$  with EGR ratio was similar to the results obtained by single particle laser ablation time-of-flight mass spectrometry (SPLAT).<sup>48,49</sup> However, the absolute values of the  $\rho_{\text{eff}}$  differed perhaps because SPLAT measurements are based on aerodynamic diameter while the DMA-APM measurements are based on electrical mobility diameter. These data provide interesting information for technologies that employ EGR ratio increases to reduce  $\text{NO}_x$  emissions, but do not enter into the advanced

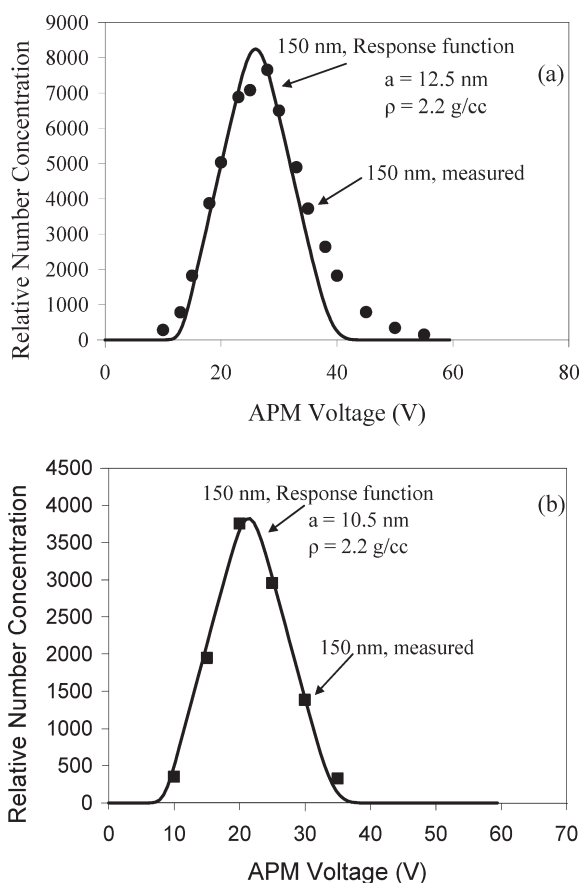


**Figure 6.** Comparison of measured and calculated DMA-APM response function for 150 nm mobility classified aggregates. The data are shown for (a) conventional mode and (b) PCCI mode. APM rotational speed = 2000 rpm. The parameter  $a$  is the primary particle radius. The height of the calculated response function is normalized for comparison. More accurate height comparison was not made in this study due to particle losses. The peak APM voltage shown above differs slightly from Gaussian fit of the measured data points shown in Figure 4. Aggregate orientation in DMA: parallel to the relative motion. Aggregate orientation in the APM is assumed random due to lesser electric field strength. Brownian diffusion is taken into account.

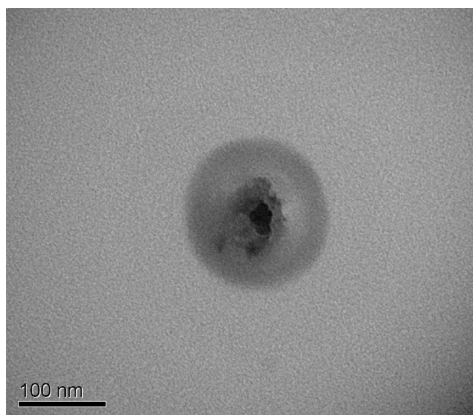


**Figure 7.** TEM image of compact PCCI particle with 100 nm electrical mobility diameter for the moderate cruise condition (1500 rpm, 2.6 bar).

combustion regime and thus rely heavily on DPF aftertreatment to reduce PM emissions.

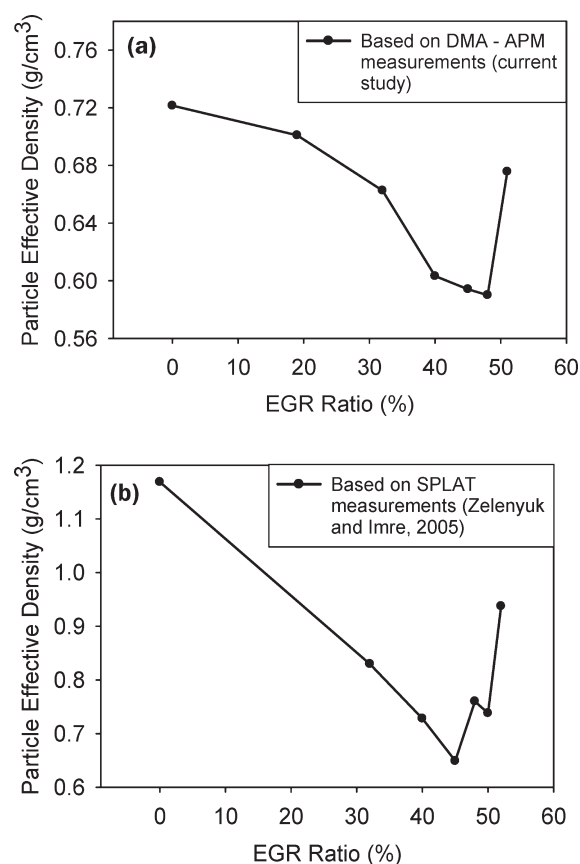


**Figure 8.** Variation in particle effective density with exhaust gas recirculation (EGR) ratio based on measurements by a) DMA-APM (current study) and (b) the single particle laser ablation time-of-flight mass spectrometer (SPLAT).<sup>49</sup> For both methods, the lowest particle effective densities were measured between 40 and 50% EGR.

## CONCLUSIONS

PCCI operation is employed to reduce engine-out emissions while maintaining fuel efficiency and may be incorporated with conventional diesel combustion in a DPF-equipped vehicle as an overall mitigation strategy. Because PCCI operation may be used in conjunction with DPF aftertreatment, the particle physical properties should be evaluated considering their effects on soot-layer porosity and hence DPF regeneration. The measured  $\rho_{\text{eff}}$  suggest that PCCI particles may form DPF filter cakes as porous as conventional diesel particles. The  $\rho_{\text{eff}}$  of PCCI and conventional diesel particles were similar for 50, 100, and 150 nm  $d_m$ . The  $d_m$  investigated are relevant since the values were characteristic of the SMPS number-size distribution. The results imply PCCI particle density would not adversely impact pressure drop across the soot layer and soot access to  $\text{O}_2$  and  $\text{NO}_2$ . In addition, the measured  $d_{\text{pp}}$  of conventional diesel and PCCI aggregates were close in value for 50, 100, and 150 nm. Although fuel and air mixing is enhanced for PCCI combustion, the probable reduction of in-cylinder local fuel-rich zones did not result in a smaller  $d_{\text{pp}}$ . For the study, typical engine operating conditions were used, but further investigation of the effect of engine speed and load may be warranted.

TEM analysis showed that most particles were present as nanoparticle aggregates which is consistent with our low  $\rho_{\text{eff}}$  measurements. This result supported the use of IA theory to include

the effect of particle morphology in the calculation of  $\rho_i$ . The  $\rho_i$  calculations were most fitting for 50 and 150 nm particles since the DMA-APM response function for aggregates compared well with the measured response function. Although the measured 100 nm response function was wider than the calculated one, the conventional diesel  $\rho_i$  was still in agreement with that reported by Park et al.<sup>2</sup> Based on these results, our analysis showed that a small spread in  $d_m$  (due to DMA transfer function) leads to a wide DMA-APM response function, which is realized as particles passing through the APM at a wide range of APM voltages resemble an apparent mass distribution. For 50 and 150 nm particles, we show that this apparent spread in particle mass is a result of the DMA-APM response function and not due to the presence of a mass distribution. A mass distribution for a given  $d_m$  can be due to several factors including the presence of particles with fractal dimension greater than two and thus deviation from the idealized aggregate model. Such a case is found for 100 nm when the measured DMA-APM response function is wider than that based on the idealized aggregate theory. Additional investigations are needed to understand the influence of particle properties on the width of the response function, and can be explored in further studies. Overall, the  $\rho_i$  results indicated a similar amount of adsorbed liquid hydrocarbons on PCCI and conventional diesel particles. Because adsorbed liquid organics can affect soot oxidation, the results suggest soot cakes formed by PCCI and conventional diesel particles would oxidize similarly in a DPF. Thus, implementing PCCI combustion in DPF-equipped vehicles may not adversely affect DPF regeneration.

## AUTHOR INFORMATION

### Corresponding Author

\*Mail: 2125 Glenn L. Martin Hall, Building 088 University of Maryland College Park, MD 20742. Phone: 301.405.4311. Fax: 301.314.9477. E-mail: mrz@umd.edu.

### Present Addresses

<sup>†</sup>EXCET, Inc., 8001 Braddock Road, Suite 105, Springfield, Virginia 22151.

## ACKNOWLEDGMENT

We thank Dr. James Bentley, Dr. Edward Kenik, and Dr. Karren More of Oak Ridge National Laboratory for their help with transmission electron microscopy analysis.

## REFERENCES

- Mädler, L.; Lall, A. A.; Friedlander, S. K. One-step aerosol synthesis of nanoparticle agglomerate films: simulation of film porosity and thickness. *Nanotechnology* **2006**, *17*, 4783–4795.
- Masoudi, M. Hydrodynamics of diesel particulate filters. SAE Paper 2002-01-1016; 2002.
- Okude, K.; Mori, K.; Shiino, S.; Moriya, T. Premixed compression ignition (PCI) combustion for simultaneous reduction of NO<sub>x</sub> and soot in diesel engine. SAE Paper 2004-01-1907; 2004.
- Kanda, T.; Hakozi, T.; Uchimoto, T.; Hatano, J.; Kitayama, N.; Sono, H. PCCI operation with early injection of conventional diesel fuel. SAE Paper 2005-01-0378; 2005.
- Akihama, K.; Takatori, Y.; Inagaki, K.; Sasaki, S.; Dean, A. M. Mechanism of the smokeless rich diesel combustion by reducing temperature. SAE Paper 2001-01-0655; 2001.
- Wagner, R. M.; Green, J. B. Jr.; Dam, T. Q.; Edwards, K. D.; Storey, J. M. Simultaneous low engine-out NO<sub>x</sub> and particulate matter with highly diluted diesel combustion. SAE Paper 2003-01-0262; 2003.

(7) Sluder, C. S.; Wagner, R. M.; Storey, J. M. E.; Lewis, S. A. Implications of particulate and precursor compounds formed during high-efficiency clean combustion in a diesel engine. SAE Paper 2005-01-3844; 2005.

(8) Storey, J. M. E.; Lewis, S. A.; Parks, J. E.; Szybist, J. P.; Barone, T. L.; Prikhodko, V. Y. Mobile source air toxics (MSATs) from high efficiency clean combustion: catalytic exhaust treatment effects. SAE Paper 2008-01-2431; 2008.

(9) Kittelson, D. B. Engines and nanoparticles: a review. *J. Aerosol Sci.* **1998**, *29*, 575–588.

(10) Park, K. H.; Cao, F.; Kittelson, D. B.; McMurry, P. H. Relationship between particle mass and mobility for diesel exhaust particles. *Environ. Sci. Technol.* **2003**, *37*, 577–583.

(11) Mathis, U.; Kaegi, R.; Mohr, M.; Zenobi, R. TEM analysis of volatile nanoparticles from particle trap equipped diesel and direct-injection spark-ignition vehicles. *Atmos. Environ.* **2004**, *38*, 4347–4355.

(12) Kirchner, U.; Scheer, V.; Vogt, R.; Kägi, R. TEM study on volatility and potential presence of solid cores in nucleation mode particles from diesel powered passenger cars. *J. Aerosol Sci.* **2009**, *40*, 55–64.

(13) Wentzel, M.; Gorzawski, H.; Naumann, K.-H.; Saathoff, H.; Weinbruch, S. Transmission electron microscopical and aerosol dynamical characterization of soot aerosols. *J. Aerosol Sci.* **2003**, *34*, 1347–1370.

(14) Okada, K.; Heintzenberg, J. Size distribution, state of mixture and morphology of urban aerosol particles at given electrical mobilities. *J. Aerosol Sci.* **2003**, *34*, 1539–1553.

(15) Barone, T. L.; Zhu, Y. The morphology of ultrafine particles on and near major freeways. *Atmos. Environ.* **2008**, *42*, 6749–6758.

(16) Ishiguro, T.; Suzuki, N.; Fujitani, Y.; Morimoto, H. Microstructural changes of diesel soot during oxidation. *Combust. Flame* **1991**, *85*, 1–6.

(17) Stanmore, B. R.; Brilhac, J. F.; Gilot, P. The oxidation of soot: a review of experiments, mechanisms and models. *Carbon* **2001**, *39*, 2247–2268.

(18) Park, K.; Kittelson, D. B.; Zachariah, M. R.; McMurry, P. H. Measurement of inherent material density of nanoparticle agglomerates. *J. Nanopart. Res.* **2004**, *6*, 267–272.

(19) Chung, A.; Lall, A. A.; Paulson, S. E. Particulate emissions by a small non-road diesel engine: biodiesel and diesel characterization and mass measurements using the extended idealized aggregates theory. *Atmos. Environ.* **2008**, *42*, 2129–2140.

(20) Lall, A. A.; Friedlander, S. K. On-line measurement of ultrafine aggregate surface area and volume distributions by electrical mobility analysis: I. Theoretical analysis. *J. Aerosol Sci.* **2006**, *37*, 260–271.

(21) Lall, A. A.; Seipenbusch, M.; Rong, W.; Friedlander, S. K. On-line measurement of ultrafine aggregate surface area and volume distributions by electrical mobility analysis: II. Comparison of measurements and theory. *J. Aerosol Sci.* **2006**, *37*, 272–282.

(22) Lall, A. A.; Rong, W.; Mädler, L.; Friedlander, S. K. Nanoparticle aggregate volume determination by electrical mobility analysis: Test of idealized aggregate theory using aerosol particle mass analyzer measurements. *J. Aerosol Sci.* **2008**, *39*, 403–417.

(23) Friedlander, S. K. *Smoke, Dust, and Haze*; Oxford University Press: New York, 2000.

(24) Dahneke, B. Viscous resistance of straight-chain aggregates of uniform spheres. *Aerosol Sci. Technol.* **1982**, *1*, 179–185.

(25) Maricq, M. M.; Xu, N. The effective density and fractal dimension of soot particles from premixed flames and motor vehicle exhaust. *J. Aerosol Sci.* **2004**, *35*, 1251–1274.

(26) Bidleman, T. F.; Billings, W. N.; Foreman, W. T. Vapor-particle partitioning of semivolatile organic compounds: estimates from field collections. *Environ. Sci. Technol.* **1986**, *20*, 1038–1043.

(27) Pankow, J. F. Review and comparative analysis of the theories on partitioning between the gas and aerosol particulate phases in the atmosphere. *Atmos. Environ.* **1987**, *21*, 2275–2283.

(28) Pankow, J. F. The calculated effects of non-exchangeable material on the gas-particle distributions of organic compounds. *Atmos. Environ.* **1988**, *22*, 1405–1409.

(29) Lall, A. A.; Ma, X.; Guha, S.; Mulholland, G. W.; Zachariah, M. R. Online nanoparticle mass measurement by combined aerosol

particle mass analyzer and differential mobility analyzer: comparison of theory and measurements. *Aerosol Sci. Technol.* **2009**, *42*, 1075–1083.

(30) McMurry, P. H.; Wang, X.; Ehara, K. The relationship between mass and mobility for atmospheric particles: a new technique for measuring particle density. *Aerosol Sci. Technol.* **2002**, *36*, 227–238.

(31) Zhou, L.; Rai, A.; Piekielek, N.; Ma, X.; Zachariah, M. Ion-mobility spectrometry of nickel nanoparticle oxidation kinetics: application to energetic materials. *J. Phys. Chem. C* **2008**, *112*, 16209–16218.

(32) Malloy, Q. G. J.; Nakao, S.; Qi, L.; Austin, R.; Stothers, C.; Hagino, H.; Cocker, D. R. Realtime aerosol density determination utilizing a modified scanning mobility particle sizer aerosol particle mass analyzer system. *Aerosol Sci. Technol.* **2009**, *43*, 673–678.

(33) Emery, M. Theoretical Analysis of Data from DMA-APM System. Masters Thesis, University of Minnesota, 2005.

(34) Rader, D. J.; McMurry, P. H. Application of the tandem differential mobility analyzer to studies of droplet growth or evaporation. *J. Aerosol Sci.* **1986**, *17*, 771–787.

(35) Stolzenburg, M. R.; McMurry, P. H. Equations governing single and tandem DMA configurations and a new lognormal approximation to the transfer function. *Aerosol Sci. Technol.* **2008**, *42*, 421–432.

(36) Mulholland, G. W.; Donnelly, M. K.; Hagwood, C. R.; Kukuck, S. R.; Hackley, V. A.; Pui, D. Y. H. Measurement of 100 and 60 nm particle standards by differential mobility analysis. *J. Res. Natl. Inst. Stand. Technol.* **2006**, *111*, 257–312.

(37) Abdul-Khalek, I. S.; Kittelson, D. B.; Graskow, B. R.; Wei, Q.; Brear, F. Diesel exhaust particle size: measurement issues and trends. SAE Paper 980525; 1998.

(38) Kittelson, D. B.; Arnold, M.; Watts, W. F. *Review of Diesel Particulate Matter Sampling Methods, Final Report*; Prepared for U.S. Environmental Protection Agency: Minneapolis, MN, 1999.

(39) Xiong, C.; Friedlander, S. K. Morphological properties of atmospheric aerosol aggregates. *Proc. Natl. Acad. Sci.* **2001**, *98*, 11851–11856.

(40) Barone, T. L.; Lall, A. A.; Zhu, Y.; Yu, R. C.; Friedlander, S. K. Inertial deposition of nanoparticle chain aggregates: Theory and comparison with impactor data for ultrafine atmospheric aerosols. *J. Nanopart. Res.* **2006**, *8*, 669–680.

(41) Zhu, J.; Lee, K. O.; Yozgatligil, A.; Choi, M. Y. Effects of engine operating conditions on morphology, microstructure, and fractal geometry of light-duty diesel engine particulates. *Proc. Combust. Inst.* **2005**, *30*, 2781–2789.

(42) Neer, A.; Koçlu, U. O. Effect of operating conditions on the size, morphology, and concentration of submicrometer particulates emitted from a diesel engine. *Combust. Flame* **2006**, *146*, 142–154.

(43) Harris, S. J.; Maricq, M. M. Signature size distributions for diesel and gasoline engine exhaust particulate matter. *J. Aerosol Sci.* **2001**, *32*, 749–764.

(44) Buonanno, G.; Dell'Isola, M.; Stabile, L.; Viola, A. Uncertainty budget of the SMPS-APS system in the measurement of PM<sub>1</sub>, PM<sub>2.5</sub>, and PM<sub>10</sub>. *Aerosol Sci. Technol.* **2009**, *43*, 1130–1141.

(45) Tobias, H. J.; Beving, D. E.; Ziemann, P. J.; Sakurai, H.; Zuk, M.; McMurry, P. H.; Zarling, D.; Waytulonis, R.; Kittelson, D. B. Chemical analysis of diesel engine nanoparticles using a nano-DMA/thermal desorption particle beam mass spectrometer. *Environ. Sci. Technol.* **2001**, *35*, 2233–2243.

(46) Virtanen, A.; Ristimäki, J.; Marjamäki, M.; Vaaraslahti, K.; Keskinen, J. Effective density of diesel exhaust particles as a function of size. SAE Paper 2002-01-0056; 2002.

(47) Parks, J.; Prikhodko, V.; Kass, M.; Huff, S. Synergies of PCCI-type combustion and lean NO<sub>x</sub> trap catalysis for diesel engines. SAE Paper 2008-01-2493; 2008.

(48) Sluder, C. S.; Wagner, R. M.; Lewis, S. A.; Storey, J. M. E. Exhaust chemistry of low-NO<sub>x</sub> low-PM diesel combustion. SAE Paper 2004-01-0114; 2004.

(49) Zelenyuk, A.; Imre, D. Single particle laser ablation time-of-flight mass spectrometer: an introduction to SPLAT. *Aerosol Sci. Technol.* **2005**, *39*, 554–568.